JOURNAL OF SOLID STATE CHEMISTRY 116, 146–156 (1995)

Hole and Electron Doping of $RNiO_3$ (R = La, Nd)

J. A. Alonso,*,[1] M. J. Martínez-Lope,* and M. A. Hidalgo*,†

*Instituto de Ciencia de Materiales de Madrid, C.S.I.C., Serrano 113, 28006 Madrid, Spain; and †Departamento de Física, Facultad de Ciencias, Universidad de Alcalá de Henares, Apt. 20, 28871 Alcalá de Henares, Spain

Received March 28, 1994; in revised form September 29, 1994; accepted October 3, 1994

The effect of hole and electron doping in the perovskites $RNiO_3$ (R = rare earths) has been studied. $R_{1-x}A_xNiO_3$ (R = La, Nd; A = Sr, Th; $0 \le x \le 0.1$) were prepared under 200 bars of oxygen and were characterized by X-ray and neutron powder diffraction, thermogravimetric analysis, differential scanning calorimetry, and resistivity measurements. The neutron data for rhombohedral $La_{0.9}Sr_{0.1}NiO_3$ or orthorhombic $Nd_{0.95}A_{0.05}NiO_3$ (A = Sr, Th) show that Sr or Th replace at random the rare-earth cations, whereas the oxygen positions remain fully occupied. NiO_6 octahedra are either contracted, in the hole-doped Sr-containing samples, or expanded, in the electron-doped Th-containing compounds, as a consequence of the decrease/increase of the Ni–O bond lengths electronically induced by doping. Accordingly, bond-valence calculations give a valence for nickel higher/lower than +3, for the Sr/Th-doped compounds, respectively. The transport properties dramatically change with respect to the undoped compounds. The metal-to-insulator transition present in $NdNiO_3$ (T = 200 K) disappears for $Nd_{1-x}Sr_xNiO_3$, which remains metallic down to 1.5 K even for the smallest doping rate (5%). This fact can be structurally related to the straightening, by 1.4° for x = 0.05, of the (Ni–O–Ni) angles, which govern the transfer integral between Ni-3d and O-2p orbitals. For $Nd_{0.95}Th_{0.05}NiO_3$ there is a suppression of the metal–insulator transition toward low temperatures (T = 132 K). Electronic factors, related to the injection of holes or electrons into the bands of the solid, are mostly responsible for the structural changes observed in these doped compounds, which cannot be explained by simple steric considerations.

INTRODUCTION

The discovery of high-temperature superconducting copper oxides has drawn new interest to noncopper transition metal (TM) perovskite oxides, in an effort to give insight which will contribute to the understanding of high-temperature superconductivity. Among the TM perovskite oxides, the majority are insulating, a few are metals and others exhibit a metal–insulator (MI) transition as a function of temperature or pressure. Torrance *et al.* (1) used a simple ionic model to explain, within the framework of Zaanen *et al.* (2), the large differences in conductivity behavior of TM oxides. However, the interpretation of the MI transitions in still complicated by the fact that, in many cases, there are simultaneous changes in the electronic, magnetic, and structural properties and it is difficult to identify the cause and the effect.

The recent report of MI transitions in the perovskites $RNiO_3$ (R = rare earths) (3) has attracted considerable attention since these transitions seem to occur without any noticeable changes in lattice symmetry, which simplifies an in-depth study of the different phenomena involved. $RNiO_3$ (R = Pr, Nd, Sm, Eu) are orthorhombic, crystallize in the $GdFeO_3$ structure (space group *Pnma*), and exhibit MI transitions below 500 K. The detailed behavior of the phase transitions was mapped out for the above-mentioned series as a function of the rare earth (4). The transition temperature (T_{MI}) decreases systematically as the rare-earth ionic size becomes larger and the subsequent distortion from the ideal cubic perovskite decreases, from Eu (T_{MI} = 480 K) to Pr (T_{MI} = 135 K). For $LaNiO_3$, the large size of La determines a less-distorted rhombohedral structure (space group $R\bar{3}c$) which, in fact, keeps its metallic character down to 1.5 K, showing no MI transition (5). $LaNiO_3$ in a Pauli paramagnetic metal, by virtue of strong Ni–O–Ni interactions (6), in which the conduction electrons seem to be highly correlated (7).

The $RNiO_3$ oxides belong to a wider family of the so-called charge-transfer-gap compounds (1, 2), having an oxygen p-like valence band and a d-like conduction band. It has been suggested that the MI transition in $RNiO_3$ is due to the broadening of the lower p-like band, which induces a closing of the charge-transfer gap (4). The width of the occupied oxygen p band is closely related to the $\theta_{Ni-O-Ni}$ angle, which governs the transfer integral between Ni-3d and O-2p orbitals. For small rare earths, the distorted perovskite structure contains bent Ni–O–Ni bonds, with a correspondingly low bandwidth which determines the existence of a charge-transfer gap and an insulating character. As the bandwidth is increased, either by increasing the size of the rare earth (i.e., decreasing the perovskite distortion and, hence, straightening

[1] To whom correspondence should be addressed.

0022-4596/95 $6.00

the Ni–O–Ni angle) or by increasing the temperature, the charge-transfer gap decreases, eventually going to zero, giving rise to a metallic state. The structural anomalies across the MI transition in $PrNiO_3$ and $NdNiO_3$ were investigated by neutron powder diffraction (8), showing a subtle shrinkage of the cell when the compounds become metallic, due to a slight decrease of the Ni–O distances driven by electronic delocalization. This effect is accompanied by coupled tilts of NiO_6 octahedra, which implies changes in the Ni–O–Ni angles ($\Delta\theta \approx -0.5°$).

The metallic state can also be induced by pressure (9, 10). A study of Nd(Pr)NiO_3 showed that T_{MI} decreases under pressure, which hence stabilizes the metallic phase. Within the framework of the charge-transfer-gap insulators, the data suggest that the primary effect of pressure is to straighten the Ni–O–Ni bond angle, leading to a broadening of the oxygen-like valence band and hence reducing the gap.

In order to broaden the knowledge of these systems, we have undertaken the preparation and study of hole- and electron-doped $RNiO_3$ oxides. The aim of this paper is to describe the different effects induced by such doping, as well as to try to establish a correlation between the structural changes observed in these phases and the transport properties. In this preliminary study, samples of composition $R_{1-x}A_xNiO_3$ (R = La, Nd; A = Sr, Th; $0 \le x \le 0.1$) were prepared and were characterized by X-ray and neutron powder diffraction, thermogravimetric analysis, differential scanning calorimetry, and resistivity measurements.

EXPERIMENTAL

Polycrystalline samples of nominal compositions $R_{1-x}A_xNiO_3$ (R = La, Nd; A = Sr, Th; $0 \le x \le 0.1$) were prepared by a liquid-mix technique. Stoichiometric amounts of analytical grade $La(NO_3)_3 \cdot 4H_2O$ or Nd_2O_3, $Ni(NO_3)_2 \cdot 6H_2O$ and $Sr(NO_3)_2$, or $Th(NO_3)_4 \cdot 5H_2O$ were solved in citric acid. The citrate solution was slowly decomposed at temperatures up to 600°C. After an intermediate treatment at 800°C, in air, the black precursor powders were heated at 1000°C under a 200-bar oxygen pressure for 12 hr. Then, the samples were cooled at 300°C hr^{-1} down to room temperature in order to favor the oxygenation of the products.

X-ray powder diffraction (XRD) patterns were obtained with CuK_α radiation in a Siemens D-501 goniometer controlled by a DACO-MP computer, by step-scanning from 10° to 100° in 2θ, in increments of 0.05° and a counting time of 4 sec each step.

The neutron powder diffraction diagrams of $La_{0.9}Sr_{0.1}NiO_3$, $Nd_{0.95}Sr_{0.05}NiO_3$, and $Nd_{0.95}Th_{0.05}NiO_3$ were collected at room temperature in the multidetector DN5 diffractometer at the Siloé reactor of the Centre d'Etudes Nucléaires, Grenoble. A wavelength of 1.345 Å was selected from a Cu monochromator. The 800 detectors covered a 2θ range of 80°, from $2\theta_i = 18°$. The counting time was about 4 hr, using about 6 g of sample.

Both X-ray and neutron diffraction patterns were analyzed by the Rietveld (11) method, using a strongly modified version (12) of the Wiles and Young refinement program (13). A pseudo-Voigt function was chosen to generate the lineshape of the diffraction peaks. In the neutron refinements, the coherent scattering lengths for La, Nd, Sr, Th, Ni, and O were respectively 8.24, 7.69, 7.02, 9.84, 10.3, and 5.805 fm.

No regions were excluded in the refinements. In cases where small amounts of unreacted NiO (with rock-salt structure) were detected in the pattern, the profile refinement of the mixture was performed. In the final run the following parameters were refined: background coefficients, zero-point, half-width, pseudo-Voight, and asymmetry parameters or the peak shape; scale factors, positional, thermal isotropic factors (overall for X-ray data), occupancy factors for the oxygen positions (neutron data only), and unit-cell parameters.

Thermal analysis was carried out in a Mettler TA3000 system equipped with a TC10 processor unit. Thermogravimetric (TG) curves were obtained in a TG50 unit, working at a heating rate of 5°C min^{-1}, in a reducing $H_2(5\%)/N_2(95\%)$ flow of 0.3 liter min^{-1}. About 50 mg of sample were used in each experiment. Differential scanning calorimetry (DSC) experiments were performed in a DSC30 unit, in the temperature range 120 to 300 K. The heating rate was 10°C min^{-1}, using about 70 mg of sample in each run.

Resistivity measurements have been performed by the standard dc four-probe method between 1.5 and 300 K. Pellets were sintered at 1000°C under 200 bar of oxygen for 12 hr.

RESULTS

1. Composition of the Samples

The undoped compounds ($RNiO_3$, R = La, Nd), prepared for comparative purposes, were obtained as black well-crystallized powders. Although the synthesis of both compounds can be carried out at atmospheric pressure (14–16) by slow decomposition of organic precursors at low temperatures (<850°C), the crystallinity of the resulting powders is, by far, much poorer than that reached under the more drastic conditions employed in this work. Moreover, all trials of introducing Sr or Th into the lattice at softer conditions led to the obtention of the competitive K_2NiF_4 phases (e.g., $La_{2-x}Sr_xNiO_4$). In this case, the use of high oxygen pressure was shown to be a key factor for the stabilization of the perovskite phases.

The Sr/Th doped samples are, for x values up to 0.1, perovskite phases showing the same symmetry as the undoped compounds, i.e., rhombohedrally distorted for the La derivatives or orthorhombically distorted for the Nd oxides. The X-ray diffraction peaks of the Sr/Th-containing phases are somewhat broadened with respect to those of the undoped samples, probably as a consequence of the structural disorder introduced by doping. For substitutional levels higher than $x = 0.1$ (A = Sr, Th), the appearance of SrO or ThO_2 as impurity phases indicates that the incorporation of Sr/Th is not total under these conditions, and the obtention of higher doping levels would probably require one to work under higher oxygen pressures.

2. Structural Changes

X-ray and neutron diffraction diagrams for La and Nd samples have been analyzed in the space groups $R\bar{3}c$ (hexagonal description) and *Pnma*, respectively. No additional peaks, which could indicate the presence of superstructures or departure from the mentioned symmetries, were observed in any of the examined diagrams. Table 1 shows the unit-cell parameters of the $R_{1-x}A_xNiO_3$ compounds, refined from the X-ray diffraction patterns. The variation of the lattice parameters and volume with the Sr/Th contents is plotted in Fig. 1.

For the La phases, the incorporation of Sr or Th leads respectively to a contraction or an expansion of the lattice. Taking into account that Sr^{2+} is larger and Th^{4+} is smaller in size than La^{3+} (Shannon's ionic radii (17) for eight-coordinated La^{3+}, 1.16 Å; Sr^{2+}, 1.26 Å; Th^{4+}, 1.05 Å), the observed behavior is opposite to that expected from steric considerations and can only be explained by assuming that the incorporation of Sr/Th is accompanied by an increase/decrease of the mean oxidation state of Ni, which could presumably shorten/lengthen the Ni–O distances.

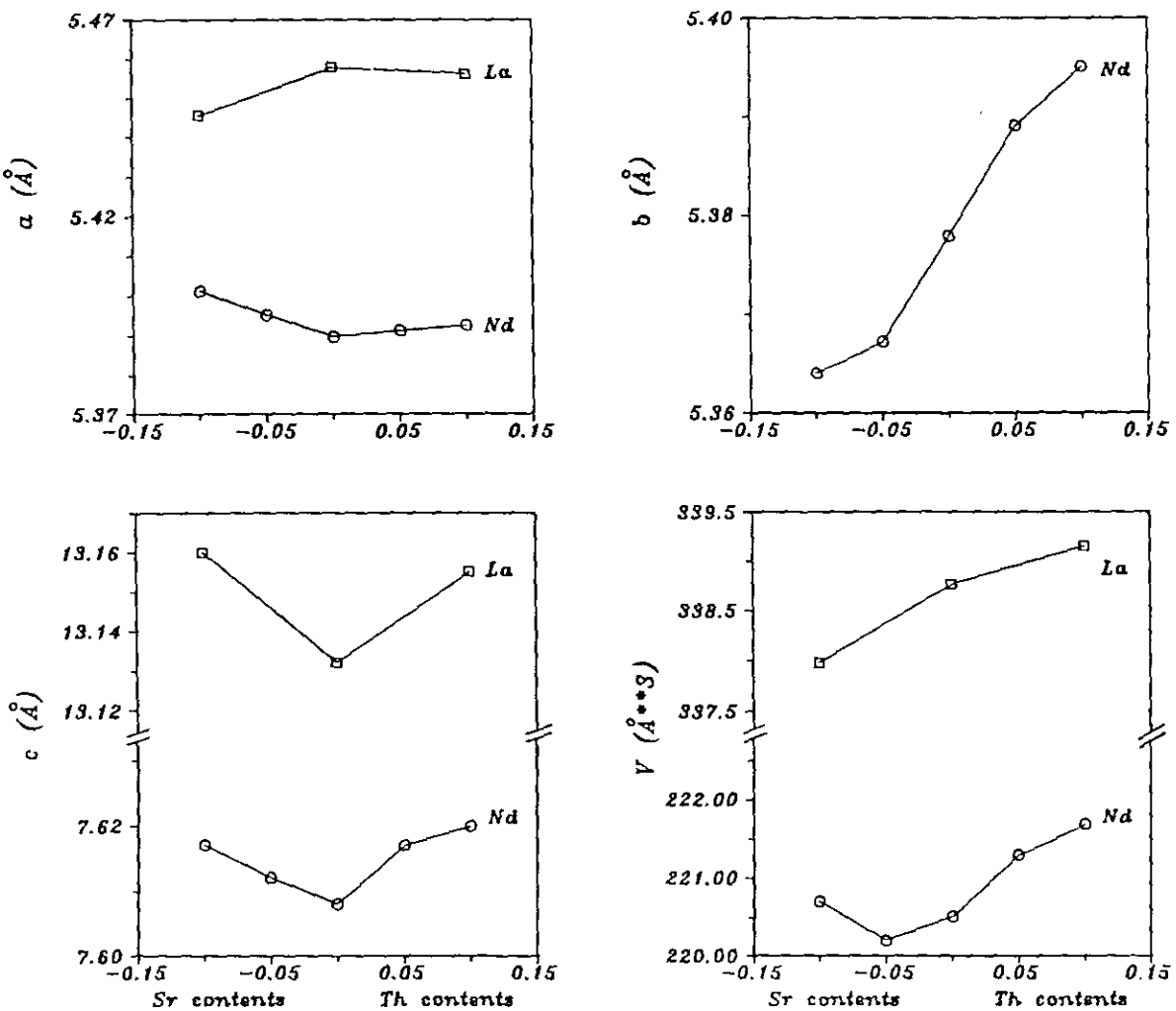

FIG. 1. Variation of the unit-cell parameters and volume of $R_{1-x}A_xNiO_3$ (R = La, Nd; A = Sr, Th) as a function of the A content, x.

TABLE 1
Unit-Cell Parameters of the $R_{1-x}A_xNiO_3$ Phases

R	A	x	a (Å)	b (Å)	c (Å)	V (Å^3)
La	Sr	0.1	5.4455(3)	5.4455(3)	13.1600(9)	337.97(5)
La	—	0	5.4578(1)	5.4578(1)	13.1323(2)	338.77(1)
La	—	0[a]	5.4573(1)	5.4573(1)	13.1462(3)	339.06(2)
La	Th	0.1	5.451(4)	5.451(4)	13.155(1)	339.15(5)
Nd	Sr	0.1	5.401(1)	5.364(1)	7.617(2)	220.7(1)
Nd	Sr	0.05	5.395(1)	5.3672(9)	7.612(2)	220.2(1)
Nd	—	0	5.3895(5)	5.3778(4)	7.6082(8)	220.51(6)
Nd	—	0[a]	5.3891(3)	5.3816(2)	7.6101(3)	220.71(3)
Nd	Th	0.05	5.3911(8)	5.3890(4)	7.617(1)	221.29(8)
Nd	Th	0.1	5.3824(9)	5.3950(6)	7.620(1)	221.68(9)

[a] Unit-cell parameters taken from Ref. (8), obtained by neutron diffraction.

For the Nd compounds (ionic size for Nd^{3+}, 1.109 Å) the variation of the unit-cell parameters is somewhat surprising: **b** increases regularly from the sample with maximum Sr content to the compound with the largest Th content, whereas **a** and **c** increase with x for both A cations. This leads to an irregular variation of the unit-cell volume. The observed behavior can be interpreted as the result of a compromise between the steric (size difference between R and A) and electronic factors (variation of the Ni–O distances) and is better understood by analyzing the local distortions of the coordination polyhedra of the perovskite.

Table 2 lists the structural parameters for $La_{0.9}Sr_{0.1}NiO_3$ and $Nd_{0.95}A_{0.05}NiO_3$ (A = Sr, Th), refined from neutron diffraction data, and Fig. 2 shows the diffraction profiles. The good agreement factors for the proposed models confirm that Sr^{2+} or Th^{4+} replace at random the rare-earth cations, i.e., occupying the 6*a* positions (La compound, $R\bar{3}c$) or 4*c* positions (Nd compounds, *Pnma*). On the other hand, the refinement of the O1 and O2 occupancy factors shows that the oxygen positions are fully occupied, within two times the standard deviations. These data suggest that, in order to maintain the electroneutrality of the crystal, the electronic state of Ni is altered by doping.

For the substitutional levels of the samples studied by neutron diffraction, the changes in the atomic parameters and, thus, in the interatomic distances, are very small but significative. Samples with a higher substitutional level (e.g., x = 0.1 for the Nd compounds) were not structurally studied because of its poorer crystallinity.

Table 3 shows, as expected, a reduction of the mean Ni–O distances in the Sr-doped samples (for both La and Nd compounds), suggesting that the formal valence of Ni has increased in these compounds. The opposite effect is observed in the Th-doped oxide, in which ⟨Ni–O⟩ is larger than that of the undoped compound.

For the La samples, a single Ni–O distance can be defined, which takes a value of 1.934(1) Å for $LaNiO_3$. The almost regular NiO_6 octahedra experience a contraction in $La_{0.9}Sr_{0.1}NiO_3$, driven by electronic factors: the Ni–O bond is shortened by 0.004 Å. The Ni–O–Ni angles increase by 1.5°, in order to keep enough room for (La, Sr) after the shortening of the Ni–O bonds. The distortion of the perovskite is, hence, reduced. Despite the straightening of the Ni–O–Ni bonds, the contraction of the lattice determines slightly smaller (La, Sr)–O distances in the doped sample, in spite of the larger size of the Sr^{2+} cations, which would demand slightly larger holes to allocate them. The electronic factors which govern the shortening of the Ni–O bonds seem to predominate, thus, on purely steric considerations. Atomic posi-

TABLE 2
Atomic and Thermal Parameters Refined from Neutron Powder Diffraction Data at 295 K for $R_{1-x}A_xNiO_3$

	R = La ($R\bar{3}c$, hexagonal description)				
A:			Sr	—	
x:			0.1	0[a]	
R, A:	6*a*	(0 0 ¼)			
B (Å^2)			0.31(4)	0.36(2)	
Ni:	6*b*	(0 0 0)			
B (Å^2)			0.20(3)	0.21(2)	
O:	18*e*	(x 0 ¼)			
x			0.5410(2)	0.5456(2)	
B(Å^2)			0.55(5)	0.55(2)	
Reliability factors[b]					
χ^2			5.0	3.5	
R_B			3.7	4.5	
	R = Nd (*Pnma*)				
A:			Sr	—	Th
x:			0.05	0[a]	0.05
R, A:	4*c*	(x y ¼)			
x			0.998(2)	0.9941(8)	0.992(1)
y			0.0312(7)	0.0343(3)	0.0380(6)
B (Å^2)			0.40(7)	0.61(3)	0.21(8)
Ni:	4*b*	(½ 0 0)			
B (Å^2)			0.33(4)	0.51(1)	0.22(5)
O1:	4*c*	(x y ¼)			
x			0.069(2)	0.070(1)	0.074(3)
y			0.495(1)	0.4921(7)	0.493(1)
B (Å^2)			1.0(3)	0.76(5)	0.8(2)
Occupancy			0.96(5)	—	1.14(7)
O2:	8*d*	(x y z)			
x			0.721(1)	0.7150(6)	0.711(2)
y			0.2811(9)	0.2842(6)	0.287(2)
z			0.0363(7)	0.0378(4)	0.0339(9)
B (Å^2)			0.26(16)	0.88(4)	0.26(16)
Occupancy			0.99(3)	—	0.94(3)
Reliability factors[b]					
χ^2			6.3	4.5	2.4
R_B			4.1	4.2	3.5

[a] Data for the x = 0 compounds are taken from Ref. (8).
[b] Defined in Ref. (13).

TABLE 3
Selected Distances (Å) and Angles (°) for $R_{1-x}A_xNiO_3$

R = La				
A:		Sr	—	
x:		0.1	0	
Ni–O	(×6)	1.930(1)	1.934(1)	
La–O	(×3)	2.500(1)	2.480(1)	
	(×3)	2.946(1)	2.978(1)	
	(×6)	2.708(2)	2.708(1)	
⟨La–O⟩		2.716(1)	2.719(1)	
Ni–O–Ni		166.71(7)	165.22(5)	
R = Nd				
A:		Sr	—	Th
x:		0.05	0	0.05
Ni–O1	(×2)	1.939(2)	1.940(1)	1.946(2)
–O2^{i}	(×2)	1.942(5)	1.939(2)	1.936(5)
–O2^{ii}	(×2)	1.930(5)	1.947(3)	1.954(5)
⟨Ni–O⟩		1.937(4)	1.942(2)	1.945(4)
$10^4\ \Delta_d$		0.069	0.030	0.144
(Nd, A)–O1		2.904(9)	2.944(4)	2.970(8)
		2.517(9)	2.496(4)	2.492(8)
		3.07(1)	3.049(7)	3.06(1)
		2.34(1)	2.360(7)	2.36(1)
–O2	(×2)	2.586(7)	2.584(4)	2.607(7)
	(×2)	2.418(7)	2.384(3)	2.396(7)
	(×2)	2.684(7)	2.677(4)	2.640(6)
⟨(Nd, A)–O⟩		2.621(8)	2.614(5)	2.617(8)
Ni–O1–Ni	(×2)	157.9(5)	157.4(2)	156.3(5)
Ni–O2–Ni	(×4)	158.6(11)	156.8(5)	157.0(10)
⟨Ni–O–Ni⟩		158.4(9)	157.0(4)	156.8(8)
O1–Ni–O2		89.4(4)	89.3(2)	90.3(4)
		90.0(5)	89.7(2)	91.3(5)
		90.0(4)	90.3(2)	88.7(4)
		90.6(4)	90.7(4)	89.7(3)
O2–Ni–O2		88.5(4)	88.7(1)	89.0(4)
		91.5(4)	91.3(2)	91.0(4)

Note. For the sake of consistency, the distances for the $x = 0$ compounds have been calculated for the atomic parameters determined by neutron diffraction in Ref. (8) and the unit-cell parameters determined by X-ray diffraction in the present work.

tions and interatomic distances for $La_{0.9}Th_{0.1}NiO_3$ are not included in Tables 2 and 3 because neutron data were not available, and the oxygen parameters obtained from X-ray data are not reliable due to the low scattering power of oxygen for X-rays.

For undoped $NdNiO_3$, the NiO_6 octahedra are also almost regular. Figure 3 shows two projections of the $NdNiO_3$ structure. The parameter Δ_d, as defined in Ref. (8), is a measurement of the distortion of the octahedra, as far as distances are concerned. For $NdNiO_3$, $\Delta_d = 0.030 \times 10^{-4}$. The distortion increases in both Sr- and Th-doped samples, $\Delta_d = 0.067 \times 10^{-4}$ and 0.144×10^{-4}, respectively. Let us examine the case of $Nd_{0.95}Sr_{0.05}NiO_3$. There is a remarkable contraction of the Ni–O2^{ii} distances (by 0.017 Å) which, together with the expansion of Ni–O2^{i}, gives rise to flattened NiO_6 octahedra. A schematic representation of such distortion is shown in Fig. 4. This effect takes place mainly on the **ab** plane of the lattice (only Ni–O2^{i} and Ni–O2^{ii} are involved). Simultaneously, the in-plane Ni–O2–Ni angles increase by 1.8°, which, as we will discuss later on, will have a dramatic influence on the physical properties of this compound.

In $Nd_{0.95}Th_{0.05}NiO_3$, an opposite distortion is observed in the **ab** plane: expansion of Ni–O2^{ii} (by 0.007 Å) and contraction of Ni–O2^{i} (by 0.003 Å). This is complemented by an increase of the Ni–O1 distances (by 0.006 Å) along the **c** axis, which is also supposed to be driven by electronic factors. The octahedra are, also in this case, flattened. In a trend to reduce the void for (Th, Nd) (Th^{4+} is smaller than Nd^{3+}) Ni-O1-Ni angles are additionally bent by 1.1°. Even under these conditions, the elec-

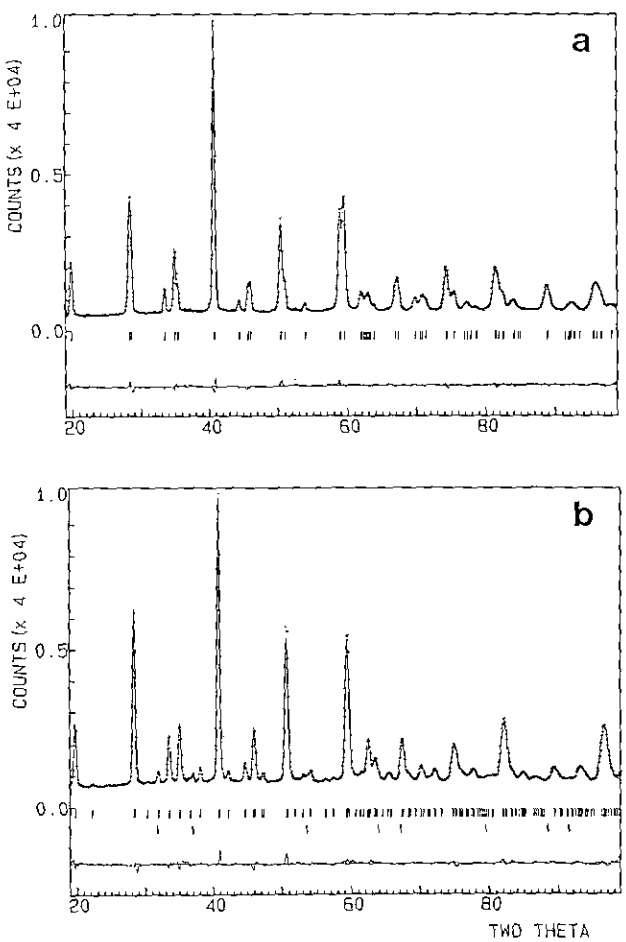

FIG. 2. Observed (crosses), calculated (solid line), and difference (at the bottom) neutron diffraction profiles for (a) rhombohedral $La_{0.9}Sr_{0.1}NiO_3$ and (b) orthorhombic $Nd_{0.95}Sr_{0.05}NiO_3$ at 295 K. The two series of thin marks indicate the positions of the allowed Bragg reflections for the main phase and NiO.

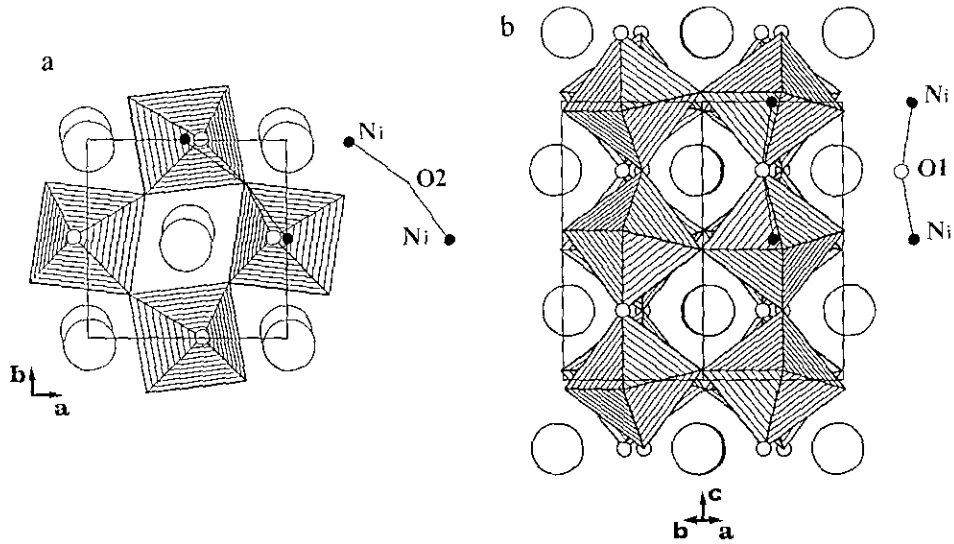

FIG. 3. Two projections of the $NdNiO_3$ structure along (a) [0 0 1], and (b) [1 1 0]. Ni–O–Ni bonds through O1 (small circles) and O2 (equatorial vertices of the octahedra) are outlined. Large circles represent Nd.

tronic factor predominates: observe that the (Nd, Th)–O distance is, in average, slightly longer, and the **c** parameter increases with respect to that of $NdNiO_3$.

3. Thermal Analysis under Reducing Conditions

3.1. Undoped $RNiO_3$ Samples

The thermal behavior of $RNiO_3$ is a reducing H_2/N_2 flow is illustrated in Fig. 5a for R = Nd. The TG curve shows two well-defined steps, starting at 280 and 410°C, respectively, with corresponding DTG peaks at 405 and 475°C. In the first one, the oxide undergoes a partial reduction to give a single phase with the composition $NdNiO_{2.5}$. During the second step, the sample completely decomposes, also by oxygen loss, giving Nd_2O_3 and Ni metal as reduction products. The total weight loss corresponds to 1.51(2) oxygen atoms per formula. The equations suggested for these reduction processes are

$$NdNiO_3 \xrightarrow{H_2} NdNiO_{2.5} + 1/2\ H_2O \qquad [1]$$

$$NdNiO_{2.5} \xrightarrow{H_2} 1/2\ Nd_2O_3 + Ni + H_2O. \qquad [2]$$

3.2. $R_{1-x}A_xNiO_3$ Samples

Figures 5b and 5c show two typical TG curves obtained in a H_2/N_2 flow, corresponding to $Nd_{0.9}A_{0.1}NiO_3$ (A = Sr, Th). A more detailed description of the thermal analysis for different rare-earths and A contents can be found elsewhere (18). The overall thermal behavior significantly differs for the Sr or Th samples.

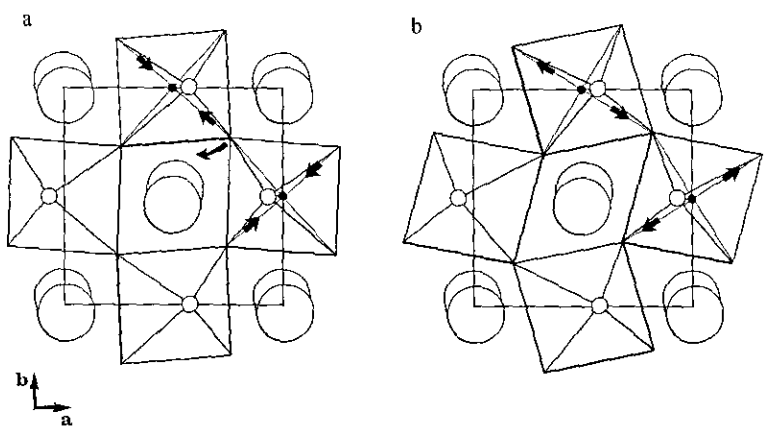

FIG. 4. Schematic view of the structure of $NdNiO_3$ doped with (a) Sr or (b) Th, projected along [0 0 1]. For the sake of clarity, the distortion of the NiO_6 octahedra on the **ab** plane has been enhanced.

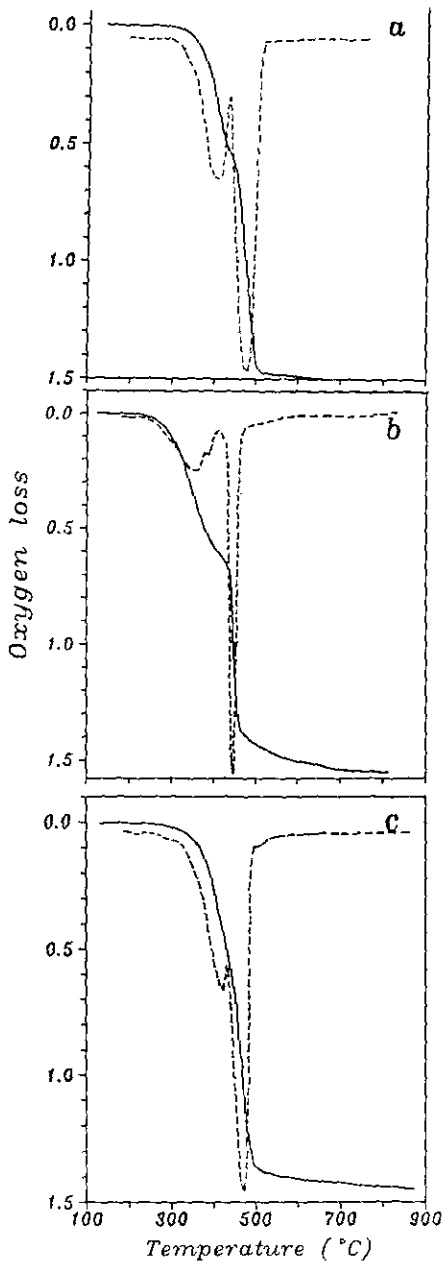

FIG. 5. TG (solid lines) and DTG (broken lines) curves obtained in a H_2/N_2 flow for (a) $NdNiO_3$, (b) $Nd_{0.9}Sr_{0.1}NiO_3$, and (c) $Nd_{0.9}Th_{0.1}NiO_3$.

3.2.1. $Nd_{0.9}Sr_{0.1}NiO_3$. Two main steps can be distinguished in the thermograms (Fig. 5b). The starting temperature of the first process, 200°C, is remarkably lower than the corresponding one for $NdNiO_3$. The DTG curve shows a shoulder that clearly reveals the presence of two overlapping processes, with maxima at 355 and 395°C. Although it is difficult to draw conclusions from the individual weight losses, due to the above-mentioned overlapping, it seems reasonable to describe them through the following equations:

$$Nd_{0.9}Sr_{0.1}NiO_3 \xrightarrow{H_2} Nd_{0.9}Sr_{0.1}NiO_{2.5} + 0.5\ H_2O \quad [3]$$

$$Nd_{0.9}Sr_{0.1}NiO_{2.5} \xrightarrow{H_2} Nd_{0.9}Sr_{0.1}NiO_{2.45} + 0.025H_2O. \quad [4]$$

Equation [3] is similar to [1], excepting that, in this case, the resulting oxygen-deficient phase contains Ni in an intermediate (II)–(III) valence, due to the Sr content. This phase seems to be unstable and immediately decomposes by further H_2 reduction, according to [4], to give a Ni(II) oxygen-deficient compound. The total weight losses for [3] + [4] are close to the calculated value of 0.55 oxygens per mole.

The second step of the thermogram, characterized by a sharp DTG peak centered at 445°C, corresponds to the total decomposition of the sample, by reduction to Ni metal, according to

$$Nd_{0.9}Sr_{0.1}NiO_{2.45} \xrightarrow{H_2} 0.45\ Nd_2O_3 + 0.1\ SrO + Ni + H_2O. \quad [5]$$

The weight loss agrees with that established for this process.

3.2.2. $Nd_{0.9}Th_{0.1}NiO_3$. The sample is stable up to 290°C (Fig. 5c). Beyond this temperature it decomposes in two steps, characterized by DTG maxima centered at 430 and 465°C. Both processes can be described by the following equations:

$$Nd_{0.9}Th_{0.1}NiO_3 \xrightarrow{H_2} Nd_{0.9}Th_{0.1}NiO_{2.55} + 0.45\ H_2O \quad [6]$$

$$Nd_{0.9}Th_{0.1}NiO_{2.55} \xrightarrow{H_2} 0.45\ Nd_2O_3 + 0.1\ ThO_2 + H_2O. \quad [7]$$

In both Sr- and Th-doped samples, the total weight losses observed after the complete reduction to Ni metal can be used to have a rough estimate of the oxidation state of Ni in the departure samples. If the full oxygen stoichiometry is assumed (as it seems to be, from the neutron diffraction data), this measurement represents an indirect method of checking the Sr or Th contents of the samples. Nevertheless, the results of such analysis must be considered as just semiquantitative, given the associated errors (up to ±0.02 oxygens) and the small doping rates of the samples.

4. DIFFERENTIAL SCANNING CALORIMETRY

Figure 6 shows the DSC curves for $Nd_{1-x}A_xNiO_3$ (A = Sr, Th; x = 0, 0.05), obtained during the heating run. The $NdNiO_3$ curve exhibits an endothermic peak centered at −72.4°C (200.8 K) corresponding to the first-order insula-

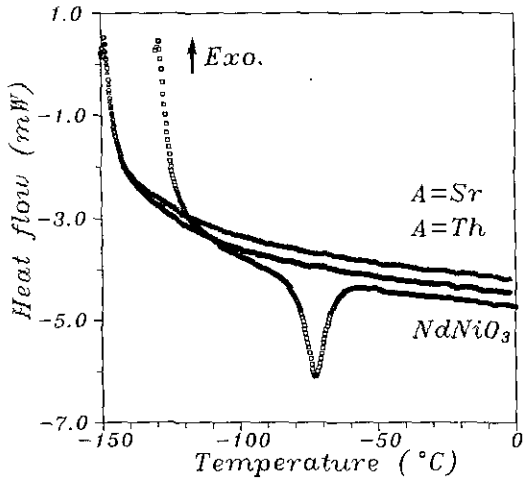

FIG. 6. DSC curves, obtained on heating, for $NdNiO_3$ and $Nd_{0.95}A_{0.05}NiO_3$ (A = Sr, Th).

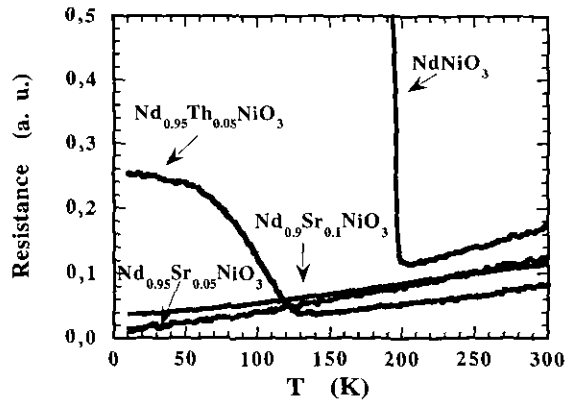

FIG. 7. Resistance vs temperature plots for $Nd_{1-x}S_xNiO_3$, recorded on heating.

tor-to-metal transition. The enthalpy variation associated to this process is ΔH = 376 J mole^{-1}. This figure is in good agreement with that reported by Granados *et al.* (19) for the heating process, ΔH = 353 J mole^{-1}. The samples doped with either Sr or Th show no peaks in the temperature range 120–300 K.

5. RESISTIVITY MEASUREMENTS

La Samples

$LaNiO_3$ behaves as a metal in the entire temperature range. The room temperature resistivity, ρ_{300} = 0.39 mΩ cm, agrees with the values reported in the literature (e.g., ρ = 0.38 mΩ cm in Ref. (20)). A metallic behavior was also observed for the Sr/Th-doped samples, with room temperature resistivity slightly higher/lower with respect to $LaNiO_3$, which could be correlated with the change in the number of carriers, induced by doping.

Nd Samples

The general behavior of the electrical resistance versus temperature, recorded on the heating process, is shown in Fig. 7. The curve of $NdNiO_3$ shows a minimum at T = 199 K (200 K in Ref. (3) or 205 K in Ref. (19)), corresponding to the well-described insulator-to-metal transition. ρ_{300} is 1.3 mΩ cm, in good agreement with the value reported by Granados *et al.* (19), 1.2 mΩ cm. For $Nd_{1-x}Sr_xNiO_3$ (x = 0.05, 0.1), the MI transition vanishes, exhibiting a metallic behavior down to 1.5 K. As for $Nd_{0.95}Th_{0.05}NiO_3$, the observed change in resistivity is less dramatic than that present in $NdNiO_3$, although two regions (metallic, semiconducting) can clearly be distinguished in the R(T) curve. The MI transition is suppressed toward low temperatures: the change of slope between the metallic and semiconducting region takes place at 132 K for $Nd_{0.95}Th_{0.05}NiO_3$.

6. DISCUSSION

The changes in the unit-cell and structural parameters as well as the particular features of the TG and DSC curves and the transport properties constitute a solid experimental basis that allows us to confirm that A atoms are introduced into the R sublattice of the studied $RNiO_3$ compounds. Neutron data and thermal analysis are in support of the full oxygen stoichiometry of these oxides. From both facts we can conclude that the Sr^{2+} or Th^{4+} substitution for R^{3+} leads to a hole or electron doping of the electronic bands of these materials.

There is a question raised concerning the origin of the subtle structural changes responsible for the differential behavior of the doped phases. In principle, these changes could be thought to be a result of the reaccommodation of the structure after the introduction into the R sublattice of A cations with different ionic sizes. The second key factor is the variation of the Ni–O distances as a consequence of the hole or electron doping of the conduction bands (of antibonding character), hence strengthening or weakening, respectively, the Ni–O bonds. Both parameters determine the tolerance factor of the perovskite ABO_3, defined as $t = d_{A-O}/\sqrt{2}d_{B-O}$ (21), which gives a rough estimate of the distortion of the structure with respect to the ideal cubic perovskite, in the framework of a purely ionic model. A rise of t would mean a decrease in the distortion of the perovskite, characterized by a reduction of the tilting angle of the BO_6 octahedra. For perovskites $RNiO_3$, it can be assumed that there is a linear relationship between small variations of the Ni–O distance and the associated variation of the Ni–O–Ni

angle (8), when purely steric factors are involved, according to

$$\Delta\theta_{\text{Ni-O-Ni}} \approx -275(d_{R\text{-O}}/\sqrt{2}d^2_{\text{Ni-O}})\Delta d_{\text{Ni-O}}. \quad [8]$$

Applying this equation to the changes observed in $La_{0.9}Sr_{0.1}NiO_3$ with respect to $LaNiO_3$, for the observed shortening of the Ni–O distances, 0.004 Å, the associated increase of the Ni–O–Ni angle should be 0.57° if steric effects predominate. Even if, qualitatively, the reduction of the Ni–O distances is, in fact, accompanied by a straightening of the Ni–O–Ni angles, the observed value, $\Delta\theta = 1.5°$, is much higher than that expected from those simple size considerations, which suggests that the electronic factors are strongly dominant in the rearrangement of the structure of this Sr-doped compound.

For $Nd_{0.95}Sr_{0.05}NiO_3$ the overall behavior is similar: there is a net opening of the Ni–O–Ni angles, which could be thought to be due to the introduction of Sr^{2+} cations, larger than Nd^{3+}. The application of Eq. [8] for the average reduction of the Ni–O distances with respect to $NdNiO_3$, 0.005 Å, gives an associated opening of the Ni–O–Ni angles of only 0.68°, based upon size considerations, whereas the observed average value is 1.4°. Again, electronic factors seem to be responsible for the additional straightening of the Ni–O–Ni angles. In addition, the situation is more complicated for the Nd samples by the fact that there is a considerable distorsion of the octahedra, the origin of which is not well understood; it is evident that that rearrangement of the structure could have been made just by reducing the tilting of smaller undistorted octahedra, with no need for distortion. Also for $Nd_{0.95}Th_{0.05}NiO_3$, despite the smaller size of Th^{4+}, Ni–O1–Ni angles are slightly opened and the void for A cations is slightly larger than that of $NdNiO_3$ (Table 3). The NiO_6 octahedra are also distorted, in an opposite way as they are in the Sr compound. Both facts also point out the predominance of the electronic factors in the rearrangement of the structure.

The formulae $R_{1-x}Sr_xNiO_3$ and $R_{1-x}Th_xNiO_3$ suggest that the formal oxidation state of Ni in these compounds is $3 + x$ and $3 - x$, respectively. Brown's bond–valence model (22, 23) allows us to have a rough estimate of the Ni valence within predefined coordination polyhedra. Table 4 lists the valences calculated for Ni, from the Ni–O distances included in Table 3, in $La_{1-x}Sr_xNiO_3$ ($x = 0$, 0.1) and $Nd_{1-x}A_xNiO_3$ (A = Sr, Th; $x = 0$, 0.05). There is an effective increment of the valence of Ni in both Sr-doped compounds, and a decrease in the Th-containing oxide. It is noteworthy to point out that, although the valence changes are smaller than expected (24), the observed trend is to increase/decrease the net Ni valence in the hole/electron-doped compounds, in spite of the distortion of the NiO_6 octahedra in which some Ni–O distances increase and some decrease with respect to $NdNiO_3$.

TABLE 4

Bond Valences (s_i) for Ni–O Bonds, Multiplicity of the Bonds [m], and Ni Valences (Σs_i) within the NiO_6 Octahedra of $R_{1-x}A_xNiO_3$

(R, A)	s_i, [m]	Σs_i
$La_{0.9}Sr_{0.1}$	0.509, [6]	3.05
La	0.503, [6]	3.02
$Nd_{0.95}Sr_{0.05}$	0.497, [2] 0.493, [2] 0.509, [2]	3.00
Nd	0.495, [2] 0.497, [2] 0.486, [2]	2.96
$Nd_{0.95}Th_{0.05}$	0.487, [2] 0.501, [2] 0.477, [2]	2.93

Note. Bond valences are calculated as $s_i = \exp[(r_0 - r_i)/B]$; $B = 0.37$, $r_0 = 1.68$ for the Ni^{III}–O^{2-} pair (from Ref. (23)). Individual Ni–O distances (r_i) are taken from Table 3.

A surprising feature of the Sr-doped samples is the metallization, with vanishing of the abrupt metal–insulator transition of the Nd-containing compounds, as shown by both resistivity and differential scanning calorimetry techniques: transport measurements indicate that Sr-doped samples behave as a metal in the entire temperature range studied. We will try to establish some simple relationships between the structural changes observed in the doped phases and the described behavior. In terms of the model suggested by Torrance *et al.* (4) for these charge-transfer-gap oxides, the metallic conductivity is reached via overlapping of the oxygen-like $2p$ valence band and the metal-like $3d$ conduction band, by assuming that this overlapping increases with temperature. The transfer integral between Ni and O orbitals is governed by the Ni–O–Ni angles, which increase with both temperature and rare-earth size, the insulator-to-metal transition taking place at "critical" values of these angles. Table 5 collects the average ⟨Ni–O–Ni⟩ angles below and above the transition for $RNiO_3$ (R = La, Pr, Nd), taken from Ref. (8), compared with those for $Nd_{0.95}A_{0.05}NiO_3$

TABLE 5

Average ⟨Ni–O–Ni⟩ Angles (°) in $RNiO_3$ (R = La, Pr, Nd), Taken from Ref. (8), Compared with Those of the $R_{1-x}A_xNiO_3$ Doped Samples

(R, A)	Insulating regime	Metallic regime
La	—	164.8 (1.5)–165.2 (RT)
$La_{0.9}Sr_{0.1}$	—	166.7 (RT)
Pr	157.6 (1.5)–157.7 (110)	158.3 (110)–158.7 (RT)
Nd	156.0 (1.5)–156.2 (170)	156.8 (215)–157.1 (RT)
$Nd_{0.95}Sr_{0.05}$	—	158.4 (RT)
$Nd_{0.95}Th_{0.05}$	—	156.8 (RT)

Note. The corresponding temperatures (K) are in parentheses.

(A = Sr, Th). For the undoped samples, the characteristic angle at which they become semiconducting clearly depends upon the nature of the rare-earth element, probably because it partially determines the energy level of the p-like oxygen bands. So far, no simple relationships have been found between the absolute values of T_{MI} and those of a simple structural parameter. However, for a given rare earth, some conclusions can be drawn from Table 5. For $NdNiO_3$, the "critical" angle is 156.8°. In $Nd_{1-x}Sr_xNiO_3$, the room-temperature ⟨Ni–O–Ni⟩ angle, 158.4°, is sufficiently above this "critical" angle, to explain the observed absence of MI transition, taking into account that the closing of such an angle by thermal effects is expected to be typically about −0.5° from RT to 1.5 K (8). In other words, the ⟨Ni–O–Ni⟩ angle for $Nd_{0.95}Sr_{0.05}NiO_3$ is 1.1° more open than that of $NdNiO_3$ at room temperature, with a correspondingly broader oxygen-like valence band which seems to be enough to keep the doped compound in the metallic regime down to 1.5 K.

The structural interpretation of the resistivity behavior observed for $Nd_{0.95}Th_{0.05}NiO_3$ is more complicated. The value of the average ⟨Ni–O–Ni⟩ angle is slightly lower than that for $NdNiO_3$ at room temperature (Table 3), which would suggest an increase in the transition temperature. However, if we look at the individual bond angles we observe that Ni–O2–Ni is, in fact, slightly more open than the corresponding room-temperature angle in $NdNiO_3$, which seems to ensure a sufficient degree of overlapping, at least on the **ab** plane, to be responsible for the metallic behavior down to a temperature even lower than T_{MI} for $NdNiO_3$. On the contrary, the Ni–O1–Ni bond (along the **c** direction) is, comparatively, extremely bent (1.1° more than the corresponding in $NdNiO_3$), which suggests a weaker overlapping along the [0 0 1] crystallographic direction. Possibly, there is no metallic conduction along this direction even at room temperature. It seems plausible that one of the effects of Th doping is the reduction of the dimensionality of this compound, as far as the transport properties are concerned. On the other hand, although the change of slope between metallic and semiconducting regions for $Nd_{0.95}Sr_{0.05}NiO_3$ is much less abrupt than that in $NdNiO_3$, complementary measurements of the Seebeck coefficients for this Th-doped sample (26) suggest that this change of slope corresponds indeed to a MI transition, characterized by a sudden change in the number of carriers. The absence of noticeable peaks on the DSC curve could be due to a lower value of the heat transfer involved during the process, owing to a less dramatic structural rearrangement upon the transition, or to the spread of the heat transfer along a wider temperature range. More experimental work is needed to complete the phenomenological description of these systems. Measurements of the Seebeck coefficient, specific heat, and magnetic properties are now in progress.

CONCLUSIONS

The RNiO$_3$ (R = La, Nd) perovskites have been hole- and electron-doped through the introduction of Sr^{2+} or Th^{4+}, respectively, into the rare-earth sublattice. The effect of doping has a dramatic influence on the physical properties, which can be related, in a qualitative way, to subtle structural changes. Hole-doped samples exhibit metallic behavior in the 1.5–300 K temperature range: for R = La, the metallic character of $LaNiO_3$ is preserved in the Sr-substituted samples; for R = Nd, the MI transition, characteristic of $NdNiO_3$, vanishes for doping rates as low as 5%, as shown by resistivity and DSC measurements. This is correlated, in both hole-doped La and Nd oxides, to the straightening of the Ni–O–Ni angles, which governs the transfer integral between Ni-3d and O-2p orbitals. Electron-doped $NdNiO_3$ behaves in a totally different, nonsymmetrical way: the abrupt resistivity change undergone by $NdNiO_3$ becomes less dramatic and it is suppressed toward lower temperatures in the Th-containing compound. The structural correlation is, in this case, more complex; only the Ni–O–Ni angles in the **ab** plane are opened enough to justify the metallic conductivity in the high temperature region. In all these doped compounds, the structural rearrangement cannot be explained by simple steric considerations. We can conclude that the electronic factors, related to the injection of holes or electrons into the bands of the solid, are mostly responsible for the changes observed in the structures of these perovskites.

ACKNOWLEDGMENTS

The authors acknowledge the financial support of the DGICYT to Project PB91-0089. They also thank Dr. José Luis García-Muñoz for the transport measurements and very helpful discussions. J. A. A. thanks the MDN group at the CEN–Grenoble for their hospitality and for the facilities at the Siloé reactor.

REFERENCES

1. J. B. Torrance, P. Lacorre, Ch. Asavaroengchai, and R. Metzger, *J. Solid State Chem.* **90,** 168 (1991).
2. J. Zaanen, G. A. Sawatzky, and J. W. Allen, *Phys. Rev. Lett.* **55,** 418 (1985).
3. P. Lacorre, J. B. Torrance, J. Pannetier, A. I. Nazzal, P. W. Wang, and T. C. Huang, *J. Solid State Chem.* **91,** 225 (1991).
4. J. B. Torrance, P. Lacorre, A. I. Nazzal, E. J. Ansaldo, and Ch. Niedermayer, *Phys. Rev. B* **45,** 8209 (1992).
5. J. B. Goodenough and P. Raccah, *J. Appl. Phys.* **36,** 1031 (1965).
6. J. B. Goodenough, *Prog. Solid State Chem.* **5,** 276 (1971).
7. J. P. Kemp and P. A. Cox, *Solid State Commun.* **75,** 731 (1990).
8. J. L. García-Muñoz, J. Rodríguez-Carvajal, P. Lacorre, and J. B. Torrance, *Phys. Rev. B* **46,** 4414 (1992).

9. X. Obradors, L. M. Paulius, M. B. Maple, J. B. Torrance, A. I. Nazzal, J. Fontcuberta, and X. Granados, *Phys. Rev. B* **47,** 12353 (1993).
10. P. C. Canfield, J. D. Thompson, S. W. Cheong, and L. W. Rupp, *Phys. Rev. B* **47,** 12357 (1993).
11. H. M. Rietveld, *J. Appl. Crystallogr.* **2,** 65 (1969).
12. J. Rodríguez-Carvajal, "FULLPROF: A Program for Rietveld Refinement and Pattern Matching Analysis." Abstracts of the Satellite Meeting of the XVth Congress of the International Union of Crystallography, Toulouse, 1990, p. 127.
13. D. B. Wiles and R. A. Young, *J. Appl. Crystallogr.* **14,** 149 (1981).
14. A. Wold, B. Post, and E. Banks, *J. Am. Chem. Soc.* **79,** 1911 (1957).
15. J. K. Vassilious, M. Hornbostel, R. Ziebarth, and F. J. Disalvo, *J. Solid State Chem.* **3,** 582 (1971).
16. J. Blasco, J. García, and M. G. Proietti, Abstracts of the XIIth International Symposium on Reactivity of Solids, Madrid, 1992.
17. R. D. Shannon, *Acta Crystallogr. Sect. A* **32,** 751 (1976).
18. M. J. Martínez-Lope, J. A. Alonso, submitted for publication.
19. X. Granados, J. Fontcuberta, X. Obradors, Ll. Mañosa, and J. B. Torrance, *Phys. Rev. B* **48,** 11666 (1993).
20. X. Q. Xu, J. L. Peng, Z. Y. Li, H. L. Ju, and R. L. Greene, *Phys. Rev. B* **48,** 1112 (1993).
21. J. B. Goodenough and J. M. Longo, *in* "Magnetic and Other Properties in Oxides and Related Compounds" (K. H. Hellwege and A. M. Hellwege, Eds.), Landolt–Börnstein, New Series, Group III, Vol. 4a, Chap. 3, p. 126. Springer-Verlag, Berlin, 1970.
22. I. D. Brown, *in* "Structure and Bonding in Crystals" (M. O'Keefe and A. Navrotsky, Eds.), Vol. 2, p. 1. Academic Press, New York, 1981.
23. N. E. Brese and M. O'Keefe, *Acta Crystallogr. Sect. B* **47,** 192 (1991).
24. This fact can be imputed to the semiempirical character of the bond–valence approach, which makes it useful mostly for comparative purposes. For instance, the calculation of the net valence of Ni in $BaNiO_3$, for which $d_{Ni-O} = 1.88$ Å [see Ref. (25)], leads to a value of 3.49 valence units, well below the expected value of +4).
25. Y. Takeda, F. Kanamaru, M. Shimada, and M. Koizumi, *Acta Crystallogr. Sect. B* **32,** 2464 (1976).
26. J. L. García-Muñoz, M. Suaaidi, J. A. Alonso, and M. J. Martínez-Lope, in preparation.